Modeling actin cable contraction

Luís Almeida, Patrizia Bagnerini, Abderrahmane Habbal

Modeling actin cable contraction

Luís Almeida[1], Patrizia Bagnerini[2], Abderrahmane Habbal[3]

[1] Laboratoire Jacques Louis Lions
Université Pierre et Marie Curie (Paris 6)
UMR 7598 CNRS
BC 187, 4 Place Jussieu
F-75252 PARIS Cédex 05, FRANCE

[2] DIPTEM
Università degli Studi di Genova
P.le Kennedy-Pad D
16129 Genova, ITALY

[3] Laboratoire J.A. Dieudonné
Université de Nice
UMR 6621 CNRS
Parc Valrose
F-06108 NICE Cédex 02, FRANCE

1 Introduction

Contraction of actin structures (in one, two or three dimensions) plays an important role in many cellular and tissue movements, both at a multicellular tissue level and at a cellular (and even intracellular) one: from muscle contraction to neural tube closure, epiboly in zebrafish embryo, the contractile ring in citokynesis, cell crawling,... examples are everywhere in the living world.

In [10], we can find a nice description of different modes of actomyosin contraction and the how it generates force for moving cells and tissues. In fact, these structures consist of meshworks of actin filaments (which are like fibers) that are cross-linked by molecular motors (Myosin II) which can make

the actin filaments slide relative to each other, thus generating deformation movements.

In this work we will be particularly concerned with the contraction of essentially 1-dimensional actin structures - by this we mean that although the actin structure actually occupies a 3-dimensional volume around an idealized 1-dimensional curve, the overall behavior of this structure can be well described (in a first approximation) as a movement (in our case a contraction) of that middle curve. This mode plays an important role at the level of a single cell (like the contractile ring that separates the two daughter cells during cytokinesis), but also at a tissue level like in wound healing in drosophila pupae and dorsal closure in drosophila embryos which we will be considering in detail in sections 2 and 3.

These latter phenomena involve the extension of an epithelial membrane to close a hole which is a very widespread process both in morphogenesis and in tissue repair. The contraction of the 1-d acto-myosin structure is known as a purse-string contraction - it makes the perimeter of the hole decrease and, eventually, the hole ends up being closed (often other actin related mechanisms play an important role in late stages of closure - we will describe some of them below). Since the cable contraction is a dynamic process, the local cable tension does not necessarily decrease when the length of the corresponding cable element decreases and the contraction may continue until the curve eventually shrinks to a point. The position of this cable, at the boundary between the hole and the epidermis defines the leading edge.

We remark that many of the ideas put forward in this paper and a good part of the modeling can be applied for studying actin structure contraction in more general settings. In fact, these curvature-type flows can be extended to arbitrary dimensions - see the closely related abstract mathematical study done in [3] which was partially inspired by some work on wound healing in drosophila pupae which we are studying in collaboration with A. Jacinto's lab. In fact, the pupal thorax epithelia seems not to be stretched and might be able to follow the movement of the cable without perturbing it too much (at least in a first approximation).

If the actin cable were isolated, i.e. free to move without having to push or pull other tissues, we can imagine it moving just by curvature.

However, in most situations we have to take into account the fact that the cable is attached to tissues that might perturb significantly the movement predicted by a simple curvature flow type model. The mechanical response of the surrounding tissues is often very complicated to describe precisely and we have to choose some simplified descriptions.

The mechanical behavior of living tissues is of viscoelastic nature, and the simplest mathematical model which may be used to describe it is the one that accounts for linear viscoelastic non-aging material. For epidermal wounds, the time scale of the closure is very long (hours) while the space scale is very small (cell characteristic length - of the order of a few μm). We may therefore

neglect inertial forces, and assume that the dynamic process of wound closure is a succession of static equilibria (quasi-static approximation). Notice that, in a quasistatic approximation, the shape of the structure that undergoes deformation is iteratively (w.r.t. time sequence) updated, and taken as an initial (at rest) shape on which the next static displacement is computed, and so on. The equilibrium equations read

$$div\sigma(\mathbf{u}) + \mathbf{f} = 0$$

with

$$\sigma(\mathbf{u}) = \sigma_0 + \sigma_{elas}(\mathbf{u}) + \sigma_{visc}(\mathbf{u})$$

and

$$\sigma_{elas}(\mathbf{u}) = \mathbb{E}\epsilon(\mathbf{u}), \quad \sigma_{visc}(\mathbf{u}) = \mu\epsilon(\mathbf{u})_t.$$

The fields $\mathbf{u}$ and $\sigma(\mathbf{u})$ are the displacements and stresses, $\mathbf{f}$ the body forces, σ_{elas} and σ_{visc} the elastic and viscous stresses, $\mathbb{E}, \mu$ are elasticity and viscosity tensors, σ_0 is the residual/initial stress, and $\epsilon(\mathbf{u}) = \frac{1}{2}(\nabla\mathbf{u} + \nabla\mathbf{u}^T)$ the linearized elastic strain.

The subscript t in the viscous stress term stands for time derivative, where time is to be understood as a counter of discrete sequence $(t_0, t_1, ...)$ of equilibria states.

Another interesting approach is the one developed in [9] which is mechanically more elaborate but is more specifically tailored for modeling dorsal closure.

In the present paper, as in [2], we neglect viscous effects, viewing the tissue as a plane homogeneous isotropic mechanical continuum which can bear traction and compression loads but not bending nor torsion. Assuming a linear elastic response of this medium, the elastic deformations are then in-plane. We also neglect the coupling term between the two planar displacements, and hence obtain a model governed by a Poisson equation with suitable boundary conditions. This model, though being mechanically questionable, turned out to be well suited from a computational viewpoint, allowing us to perform an efficient parameter identification task in [2], and yielding a good predictor model.

In this work we concentrate on the treatment of non-homogeneous forces, i.e. non constant boundary terms which can be associated with having a non-uniform cable, internal pull or zipping force which may result from the non-uniformity of the boundary cells or of the connective tissue as described below. We will implement it in this simple mechanical setting, but the techniques we develop can be extended to more complex situations.

In section 2 we will start by presenting a simple model for simulating the movement of a cable that is attached to an external epithelial tissue, like in the case of the boundary (leading edge) of an epidermal wound. It will be the basis upon which all the other models will be built by adding

extra terms that describe the particular situation considered. Based on the previous discussion, it will consist of a curvature term to describe the cable contraction and a Laplacian to describe the response of the surrounding epithelia that the cable will have to drag when it contracts to close the middle hole.

In more general situations, after the tissue is wounded, a scab is formed covering the wounded surface and below it and keratinocytes start migrating from the cut edges to repair the epidermal layer. In adult wounds, the main mechanism for this movement is lamellipodal crawling, i.e. the cells in the first rows extend lamellipodia (which are essentially two dimensional actin structures) that attach to extracellular matrix and pull the epithelium forward into the wounded area. Beneath, at the dermal level, activated fibroblasts proliferate and give rise to the granulation tissue which actively contracts helping the advance of the wound edges. Both these contributions will be taken into account by considering that there is an active pull (of the lamellipodia or the connective tissue) on the leading edge that moves it inwards to close the hole.

In our mathematical model, this will lead us to consider an extra term that will be added to the curvature flow one associated to actin cable contraction: we will simulate this pulling force as a normal force, which had been taken to be constant in [1], but which will now be allowed to change along the leading edge to be able to account for non-homogeneity of material properties or biological behavior.

Finally, we consider one more extension of the model: we will study dorsal closure in a non uniform setting. Here, we will keep the normal pull term as used in the previous case, but which will now be associated to amnioserosa contraction, and will consider a new term associated to the zipping between the two margins of the leading edge which plays an essential role in this phenomenon. Again, unlike what we had done in [2], the zipping coefficient no longer needs to be constant thanks to our new approach in the simulations.

2 Mathematical model

2.1 Basic model

As was shown in [16] in the few minutes that follow a laser (or a mechanical) wounding of the epidermis of a drosophila embryo, filamentous actin and myosin II are concentrated inside the adjacent cells (just next to the cellular membranes directly exposed to the wound). This gives rise to a local acto-myosin cable element. Such intercellular cable elements are anchored into adherens junctions between neighboring cells (which are locally reinforced) and are thus all connected forming a supra-cellular acto-myosin cable that encircles the wound. This cable structure is being contracted all the time

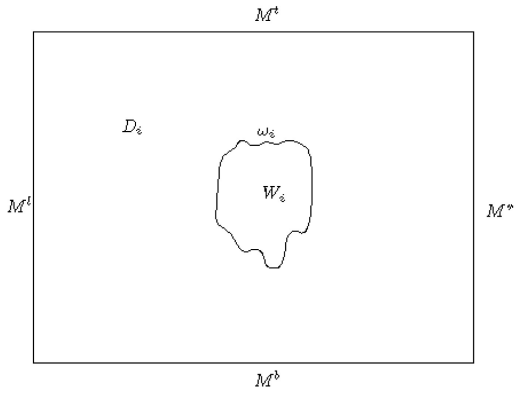

Figure 1: Computational domain.

thanks to the action of the myosin II molecular motors and is thus under tension. The contraction of this cable reduces the wound's perimeter and helps it close by the purse-string mechanism. As we mentioned before, this mechanism is used not only for wounds in fly embryos but plays an important role in many situations and different species (see [11] for a review).

In our model, the acto-myosin cable tension gives rise to a force that is proportional to the curvature (in the spirit of what was described in [5] and extended in [2]). Supposing that the leading edge is parameterized in the positive (counter-clockwise) direction, this term will be described by a normal force which is proportional to the local curvature of the leading edge at each point. It points towards the exterior of D_i (i.e. towards the interior of the wound W_i) at the points of positive curvature and towards the its interior at points of negative curvature.

In this work we will use this full curvature approach although, as discussed in [3], the experimental work done with A. Jacinto's lab on pupal wounds indicates that one should just take the positive part of this curvature in that case - this might be a more general behavior to prevent the wound from expanding after the cable is assembled (see also the discussion in [4] concerning boundary convexity and cable formation which is done in the context of zebrafish epiboly but which might convey a quite general principle).

Our simulation domain is a rectangle, M, which contains our wound W (the part no longer occupied by the epidermis). The part of the domain occupied by the epidermis is $D = M \setminus W$. The wound W (and therefore also D) change in time. In our quasistatic approach this corresponds to having a sequence of wound positions W_i and associated domains $D_i = M \setminus W_i$ corresponding to the successive time steps which are labeled by the index i. The leading edge will be denoted by $\omega_i = \partial W_i$.

We will take the same type of boundary conditions we had chosen in [1] and [2]: they allow us to consider an applied external force - this is useful for considering the anisotropic epithelial tension in embryonic wound healing or in dorsal closure. Here, to study the cases where the external tissue is not under a particular tension (the wound healing examples given), we just set that force to zero, and in dorsal closure take it into consideration. These boundary conditions correspond to taking Dirichlet boundary conditions on the lateral sides of the boundary of our simulation domain (the rectangle M) and constant Neumann conditions on its top and bottom sides. Therefore, in our simple model we will assume that at each time step i, the corresponding displacement field $\mathbf{u}_i$ will satisfy

$$\begin{cases} -\Delta \mathbf{u}_i = \mathbf{0} \ \text{ in } \ D_i, \\ \\ \mathbf{u}_i = 0 \ \text{ on } M^l \cup M^r, \\ \\ \dfrac{\partial \mathbf{u}_i}{\partial n}(q) = \mathbf{0} \ \text{ on } M^t \cup M^b, \\ \\ \dfrac{\partial \mathbf{u}_i}{\partial n}(q) = f_{cable}(q,i)\kappa(q,i)\mathbf{n}(q,i) \text{ on } \omega_i \ . \end{cases} \tag{1}$$

where $\mathbf{n}(q,i)$ is the external unit normal to ∂D_i at point q, $\kappa(q,i)$ is the curvature of ω_i at point q and $f_{cable}(q,i)$ is the function associated with the intensity of the cable tension at each point $q \in \omega_i$ of the leading edge and each time step i. Here, M^l , M^r , M^t and M^b are, respectively, the left, right, top and bottom sides of the simulation rectangle M.

We notice that allowing for a more general operator (instead of the Laplacian) and more general time and space dependence of the forces opens many possibilities to make this model evolve and adapt to many different settings. We use bold face letters for $\mathbf{u}_i, \mathbf{n}$ and $\mathbf{0}$ to make it clear that all these quantities are vectors (two-dimensional, in the present case).

Once $\mathbf{u}_i$ is obtained, we consider its restriction to the leading edge ω_i and displace this boundary (using a level set method) to obtain ω_{i+1}. More precisely, as will be described in section 3, we compute the solution $\mathbf{u}_i$ of our equation in the domain D_i by using finite element methods on a triangular mesh. We obtain a vector field $\mathbf{u}_i$, which is used as a velocity vector in the level set method in order to move ω_i and obtain ω_{i+1}.

The position of ω_{i+1} obtained also defines the new wound position (the domain enclosed by ω_{i+1} is the new position of the wound, W_{i+1}) and the new epidermal domain $D_{i+1} = M \setminus W_{i+1}$ which will be used in the following step to solve equation (1) in order to obtain $\mathbf{u}_{i+1}$, and so on.

As described above, the model in this section is just built by adding to our curvature flow boundary term, the fact that the cable has to pull the epidermis, whose response is described by a Laplacian in this basic approach.

The cable tension appears as a Neumann boundary condition on the leading edge ω_i (which is where this force acts).

2.2 Extension 1 : non homogeneous wound healing

As we saw before, in wounds we often have lamellipodal crawling and granulation tissue contraction to help the closure. To take this into account, we propose a first variant of the basic model where a new Neumann boundary term is added on the leading edge - it corresponds to a uniform normal force pointing towards the exterior of D_i, i.e. the interior of the wound W_i.

Our equation becomes

$$\begin{cases} -\Delta \mathbf{u}_i = \mathbf{0} \ \text{ in } \ D_i, \\ \\ \mathbf{u}_i = 0 \ \text{ on } M^l \cup M^r, \\ \\ \dfrac{\partial \mathbf{u}_i}{\partial n}(q) = \mathbf{0} \ \text{ on } M^t \cup M^b, \\ \\ \dfrac{\partial \mathbf{u}_i}{\partial n}(q) = f_{cable}(q,i)\kappa(q,i)\mathbf{n}(q,i) + f_{pull}(q,i)\mathbf{n}(q,i) \ \text{ on } \omega_i \ . \end{cases} \tag{2}$$

where $f_{pull}(q,i)$ is the function describing the intensity of the inwards pull at each point $q \in \omega_i$ of the leading edge and each time step i.

We notice that in this work we no longer require $f_{cable}(q,i)$ and $f_{pull}(q,i)$ to be constant parameters, as was the case in our previous work [2]. This enables us to deal with situations where the cable properties are no longer uniform like, for instance, the ones where certain proteins that are important for cable or lamellipodia formation and contraction are affected using an engrailled-gal4 driver that restricts their normal expression to certain bands (corresponding to half-segments) along the anterio-posterior axis of the fly (see [16] and the discussion below).

2.3 Extension 2: non homogeneous dorsal closure

As one further illustration of the possible applications of extended versions of our model, we will use it to study dorsal closure in a non-homogeneous setting.

Dorsal closure is an extensively studied drosophila embryogenetic movement which starts about ten hours after the drosophila egg is laid. During embryogenesis, drosophila embryos undergo epithelial folding and unfolding, which leads to a hole in the dorsal epidermis, transiently covered by a layer of large and thin cells called the amnioserosa (which, as we will describe below, plays in dorsal closure a role equivalent to that of the connective tissue in wound healing). The cells in the dorsal-most row of the lateral epidermis

are called the leading edge cells - these cells form the boundary of the lateral epidermis and they accumulate actin and myosin at their dorsal-most edge to form a contractile actomyosin cable just like we saw above for wound-healing (this cable is located at the boundary of the lateral epidermis and defines the leading edge). The hole is roughly shaped like an ellipse with major axis along the dorsal midline of the organism - which is along the anterior-posterior (AP) axis. By convention, we will consider our embryo with the anterior on the left, the posterior on the right and a horizontal AP axis. The anterior and posterior ends of the hole are called the canthi - the leading edge has a rather singular geometry at these points. The canthi separate the leading edge (also denoted ω_i as before) into two halves - the top margin, denoted ω_i^t, and the bottom margin, ω_i^b (in fact, in the original geometry of the embryo, these correspond to the right and left margins, respectively).

Dorsal closure consists of the migration of lateral epidermal cells towards the midline covering the amnioserosa in a couple of hours. This process does not involve any cell division but only a coordinated reorganization and contraction of the actomyosin cytoskeleton in different populations of epithelial cells. Moreover, the leading edge cells extend actin protrusions, called filopodia, that intertwine near the canthi drawing the two margins towards each other and knitting them. It is like the canthi advanced towards the middle of the opening behaving like zippers - which is why this phenomenon is called zipping. As the two margins merge during dorsal closure the cells from each side of the epidermis that meet end up establishing permanent junctions similar to those between the other epidermal cells. At that stage the actin corresponding to the cable segment they contained is de-polymerised and in the end there is no trace remaining of the cable.

In Dorsal closure zipping plays a very important role and has to be taken into account. In general, as discussed in [1], we can model the zipping force by a term of the type

$$Z(x) = \int_\omega f(x,y)\frac{y-x}{|y-x|}dy \quad \text{for all } x \in \omega \ , \tag{3}$$

where ω is the leading edge and we can assume that f depends on the distance between the points ($|x-y|$). Indeed, we can write, $f(x,y) = g(|x-y|)h(x,y)$, where the function $g : \mathbb{R}^+ \to \mathbb{R}$ has compact support inside $|x-y| < 2L$, where L is the maximum length of filopodia in the situation considered (it should depend on the particular fly line used).

In dorsal closure, we have particular geometry and behavior that simplify modeling the zipping force: there is apparently no zipping between points in the same margin (at least in the wild type setting and the genetically modified settings we observed), which implies that $f(x,y) = 0$ if x and y belong to the same margin (thus, the integration in (3) will only be over the opposite margin).

Moreover, the epidermis of the embryo is divided into 14 segments separated by sharp boundaries, each of them constituted by anterior and posterior half-segments (the cells of the former express a protein called patched and those of the latter one called engrailed). We could track segment and parasegment boundaries (the latter being those that separate anterior and posterior cells inside each segment) during dorsal closure, in the spirit of what will be done in the numerical simulations presented below) and see that physical points on the leading edge move vertically, i.e. orthogonally to the AP axis (see [2], figure 2).

Here, we will consider that we have a vertical zipping force which is supported in the part of the leading edge where the vertical distance between the two margins is smaller than $2L$. The subset of the leading edge where this condition is true is denoted Z_i.

In [5] four forces were described as acting on the mid-point of the leading edge (supposed to be the union of two arcs of circle in their model), namely the two that we considered in the wound healing model presented above (cable tension and internal pull) and two others:

> Epithelial resistance - since mitosis is mostly blocked at this stage, there is no significant production of new cells to cover the extra area as the LE advances - the epithelial cells are just being stretched and resist the movement yielding a resistive force. We simulate it in (4) by adding constant Neumann boundary conditions (pulling out) on the top and bottom boundaries of the simulation rectangle, as we had done in [2].
>
> The zipping force described above - it acts near the canthi where the leading edges on either side are at filopodial reach of each other (the filopodia have a maximum length of about 10 micrometers for wild type embryos). It is simulated using a Neumann boundary condition supported in the zipping set Z_i and pointing verticaly down on the top margin and down on the bottom one.

We notice that in dorsal closure, the inwards pulling force is associated to amnioserosa contraction that is created by the active contraction of the apical surface of amnioserosa cells eventually associated with apoptosis of these cells ([15]). In our first simple model we simulate this contribution by a constant normal force although it is known that at small time-scales its behavior is considerably richer (see [14]).

Our equation becomes

$$\begin{cases} -\Delta \mathbf{u}_i = \mathbf{0} \ \text{ in } \ D_i, \\ \mathbf{u}_i = 0 \ \text{ on } M^l \cup M^r, \\ \dfrac{\partial \mathbf{u}_i}{\partial n}(q) = C_1 \mathbf{n}(q) \ \text{ on } M^t \cup M^b, \\ \dfrac{\partial \mathbf{u}_i}{\partial n}(q) = f_{cable}(q,i)\kappa(q,i)\mathbf{n}(q,i) + f_{pull}(q,i)\mathbf{n}(q,i) \ \text{ on } \omega_i \setminus Z_i \ , \\ \dfrac{\partial \mathbf{u}_i}{\partial n}(q) = f_{pull}(q,i)\mathbf{n}(q,i) + f_{zip}(q,i)\mathbf{v}(q,i) + \ \text{ on } Z_i \ . \end{cases} \tag{4}$$

where $f_{zip}(q,i)$ is the function that is associated with the zipping force at point q and step i and $\mathbf{v}(q,i)$ is the vertical unit vector pointing downwards on the top margin, ω_i^t, and upwards on the bottom one, ω_i^b. As above, M^l , M^r , M^t and M^b are, respectively, the left, right, top and bottom sides of the simulation rectangle M.

3 Numerical simulations

3.1 Numerical method

In this work, unlike in [2], we consider non homogeneous coefficients, i.e. the coefficients need not be constant in the entire boundary of the wound or in the entire leading edge in dorsal closure. More precisely, the method implemented here is particularly adapted for the case of piecewise constant coefficients, which are allowed to take different values in a finite number of regions along the boundary. This setting is very natural to model a certain number of widespread situations like the ones presented below. It is nearly custom made for dealing with changes in the tissue properties that are obtained using the UAS-Gal4 system where the expression of a particular gene is modified in a pre-defined region like for instance the engrailed or the patched half segments mentioned in the previous section - this is a widespread technique in fly developmental biology (see, for instance, [16] and [6] for applications in the settings considered here) and we had it in mind when developing this approach. It is thus natural to follow the N material points that mark the boundaries between the regions having different properties - we will use a Lagrangian approach to follow the way they propagate as our boundary evolves in time.

Let ω_1 be the initial contour. We single out N points in ω_1, which divide the boundary in regions having different coefficients. Let $P(1)$ be this set of initial points. For each time step $i \geq 1$, we obtain a new contour

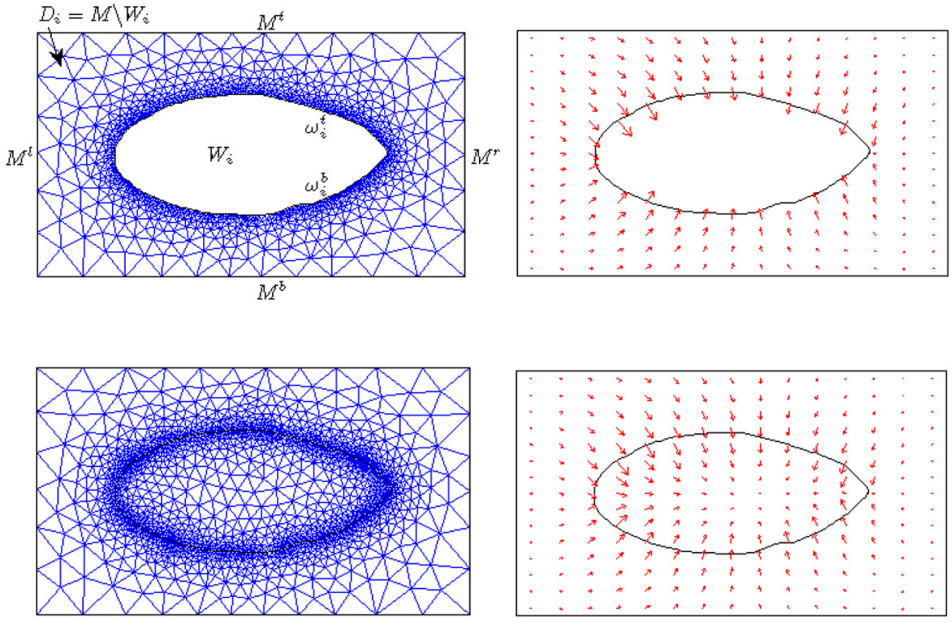

Figure 2: Example of a computed solution $\mathbf{u}_i$ alone (top right) and together with its associated extension $\mathbf{u}_i^{int}$ (bottom right) and the corresponding computational meshes (left).

ω_{i+1} and set of points $P(i+1)$ from the previously computed ones ω_i and $P(i) = \{\mathbf{p}_1(i), \ldots, \mathbf{p}_N(i)\}$ by the following algorithm.

Step 1.

We compute the solution of problem (1), (2), (4), or another extension modeling the situation under consideration), in the domain $D_i = M\backslash W_i$ by using finite element methods on a triangular mesh (using comsol multiphysics software, http://www.consol.com). We obtain in this way a displacement field $\mathbf{u}_i$, which is used as a velocity vector field to move ω_i (see figure 2) in order to obtain the new position of the boundary ω_{i+1}. We use the coordinates of the points belonging to $P(i)$ to identify the parts of ω_i with different coefficients, in order to impose appropriate boundary conditions in the problem.

We then construct an extension velocity which, starting with the velocity prescribed at the interface, builds a suitable velocity field everywhere in the rectangular domain. This extension (necessary for performing level set methods, see step 2) is in general not straightforward. In our case there is a natural harmonic extension in the domain inside the inner boundary ω_i by solving

$$\begin{cases} -\Delta \mathbf{u}_i^{int} = 0 \ \text{ in } \ W_i, \\ \mathbf{u}_i^{int} = \mathbf{u}_i \ \text{ on } \omega_i. \end{cases} \tag{5}$$

We obtain in this way an extension of the original vector field $\mathbf{u}_i$ (which for simplicity we will still denote by $\mathbf{u}_i$) to the entire rectangular domain M, see Figure 2.

Step 2. Having obtained $\mathbf{u}_i$, in order to perform the evolution of contour ω_i, we use level set methods, a set of popular algorithms for tracking and simulating the motion of dynamic surfaces in many fields as image processing, computational fluid dynamics, seismic analysis and material science. The level set methods consist in implicitly representing the front ω_i as the zero level set of a function $\Phi : \mathbb{R}^2 \times \mathbb{R}^+ \to \mathbb{R}$, solution of the Hamilton-Jacobi equation (HJ)

$$\begin{cases} \partial_t \Phi(x,t) + \mathbf{u}_i(x) \cdot \nabla \Phi(x,t) = 0 \ \text{ in } \ M \times [0,T], \\ \Phi(x,0) = \Phi_i(x) \ \text{ in } \ M, \end{cases} \tag{6}$$

where $\mathbf{u}_i$ (solution of our original problem extended using (5)) gives the direction of front propagation and ∇ denotes the spatial gradient (see Figure **??**). For the first initial contour, the function $\Phi_1(x)$ is obtained by computing the signed distance to the front ω_i (positive at the interior of ω_i), whereas for the following contours, $\Phi_i(x)$ is the solution of (6) computed at the previous time step $i-1$.

We use an Eulerian method instead of particle (Lagrangian) method since changes of topology are naturally handled and surfaces automatically merge and separate; this is particularly useful in the engrailed-spastin application where there are some changes of topology (see figure 9).

We solve the HJ problem (6) on a regular cartesian grid by using a second order numerical finite differences scheme both in space and in time. The value of $\mathbf{u}_i$ in the regular grid is computed by interpolating $\mathbf{u}_i$ on a triangular mesh. Due to the hyperbolic character of equation (6), upwinded approximations or artificial viscosity must be used in order to maintain stability. We perform spatial discretization by using an upwind second order Essentially Non-Oscillatory (ENO) scheme ([13], [8, chap. 3]). The time discretization is treated by a second order total variation diminishing Runge-Kutta scheme. The level set methods are implemented by using the Matlab toolbox of Ian M. Mitchell ([12]) (http://www.cs.ubc.ca/˜ mitchell).

Step 3. We displace the set of points $P(i)$ (belonging to ω_i) by using the vector field $\mathbf{u}_i$ in order to obtain a new set of points $P(i+1)$ belonging to ω_{i+1}. At each time step i, this set of points partitions our boundary curve ω_i into different segments where the coefficients are constant. Let $\mathbf{p}_j(i) = (x_j(i), y_j(i)),\ j = 1, \dots N$ be the coordinates of the points of the set $P(i)$ at time step i. We compute the coordinates $\mathbf{p}_j^{i+1}$ of the points in $P(i+1)$ at time step $i+1$ by solving (with a fourth order Runge-Kutta scheme) for each of them, the following boundary value problem (we will be

solving this problem N times, with a different initial condition for each j)

$$\begin{cases} \mathbf{p}'(t) = \mathbf{u}_i \ \text{ in } \ [0,T] \\ \mathbf{p}(0) = \mathbf{p}_j(i) = (x_j^i, y_j^i). \end{cases} \tag{7}$$

In the paper [2], to take advantage of the linearity, at each time step i, ω_i is chosen as the experimental contour extracted from the image number i of the film. In the present paper we perform simulations without using experimental data and therefore we always take as ω_i the previously computed contour.

As described above, in the case of the dorsal closure, filopodia from cells on the opposing margins first meet at the canthi and interdigitate, then contract and their transient adhesions are changed into permanent adhesions with the formation of adherens junctions. The vertical zipping force used to simulate this phenomenon is able to bring the opposing epithelia close to each other, but is not adapted to describe the establishment of adherens junctions and the following disappearance from the leading edge of this part of contour. This deficiency in not particularly penalizing in [2] since there at each step we restart from the experimental contour and the small, not perfectly closed part of the canthi is negligible.

In this work, on the contrary, we use the computed contour to pass from one quasi-static equilibrium contour to the next one, and thus we need to introduce a procedure to eliminate this effect and avoid having it propagate through successive simulation steps. We do so by defining the parts of the leading edge where opposing epithelia are beyond the zipping model and into the adhesion phase, to be the regions where the vertical distance between the two margins is smaller than a certain appropriately chosen (small) positive constant. In these areas, after computing on the regular grid the solution Φ_{i+1} of (6), we replace the positive value of Φ_{i+1} inside ω_i by a small negative value. Therefore, the zero level sets of Φ_{i+1} are displaced towards the middle of the wound and away from these regions, see Figure.

3.2 Some examples in non homogeneous wound healing

The numerical experiment shown in figure 3 is presented as a reference case. It corresponds to the successive positions of the boundary ω_i for our basic model (based on equation (1)) with constant cable tension $f_{cable}(q,i) = 0.01, \forall i = 1 \dots N, \ \forall q \in \omega_i$. The initial position is an ellipsoid which is symmetric relative to the verical and the horizontal axis passing through its center of mass, c_m (computed supposing we have a ellipsoid with uniform density). We see that it will shrink in successive time steps until eventually closing around c_m. In this case, the symmetry of the ellipsoid (relative to the central vertical and horizontal axis) is conserved all along the evolution.

In figure 4, we consider the case where, starting from the same initial curve, the actin cable contraction is different between upper and lower sides

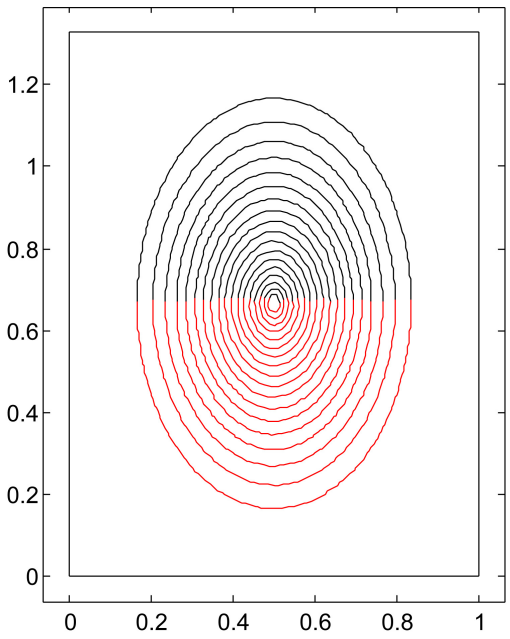

Figure 3: Initial wound is an ellipsoid subject to homogeneous cable tension, i.e. the magnitude of f_{cable} is constant, equal to 0.01, on both upper (marked in black) and lower (marked in red) halves of the successive curve positions - which are all ellipsoids.

of the wound, resulting in a faster front velocity on the part where the tension is higher: the upper portion of the successive contours (in black) which are obtained by propagating the upper half of the initial ellipsoid. Compared to the reference case in figure-3, one can observe that the final closure occurs above the horizontal axis containing the center of mass of the initial contour - vertical symmetry is naturally broken in this case.

The Cassini oval experiment in figure 5 shows that, as expected, the cable contraction flows away the negative curvature portions of the leading edge very rapidly, making it convex. It then follows very similar dynamics as the one observed in figure 4 where the values of f_{cable} are the same as here.

In figure 6 we start from a more realistic initial geometry and we consider the two terms described in subsection 2.2, namely, the cable tension term as in the previous examples (which here are taken as uniform, $f_{cable} = 0.02$), plus the interior pull which is supposed to be active only on the red part of the boundary ($f_{pull} = 0.03$ in this portion).

We notice that, for simplicity, in these examples we never considered a time dependence (where time is the index i as described before) of the values of the different terms, but the model allows such dependence.

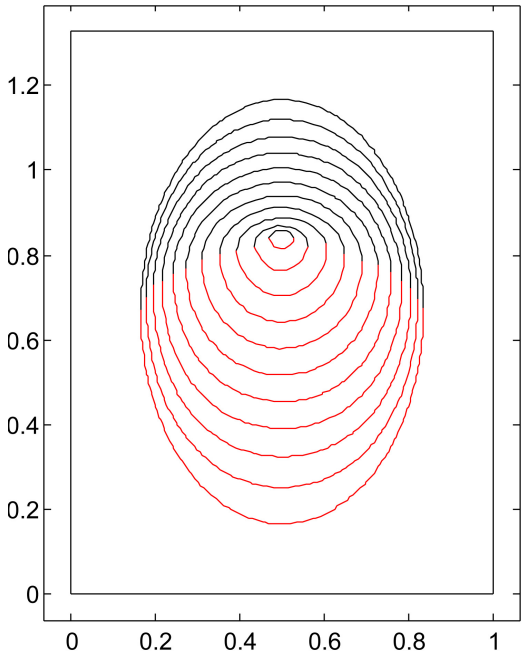

Figure 4: Initial wound is the same ellipsoid as in figure 3, but now the magnitude f_{cable} is equal to 0.02 on upper side (black) and to 0.04 on the lower side (red) - we are no longer in a constant cable tension setting and the red (higher tension) portion moves faster.

3.3 Some examples in non homogeneous dorsal closure

In this subsection we will consider two examples where we change the magnitude of the zipping force - the extra term that we introduced in subsection 2.3 to model dorsal closure. As before, we start by a standard situation: in figure 7 you can see the evolution obtained using our approach (based on equation 4) with uniform zipping coefficient of a realisitic native dorsal closure initial contour.

Next, in figure 8 we present a simple non-homogeneous case where we suppose that the value of f_{zip} is lower close to the left-hand canthus than to the right-hand one - this leads to this latter one advancing considerably faster than the former, as expected. Consequently, the wound closes towards the left side when compared to the closure shown in figure 7 where it closes near the center.

Finally, in figure 9 we consider the case where the values of f_{zip} change along vertical stripes in the initial contour. These different portions of the initial contour are then propagated as described above to simulate the movement of the material points and f_{zip} remains zero while the point is far away from the opposite margin but takes the value corresponding to the original

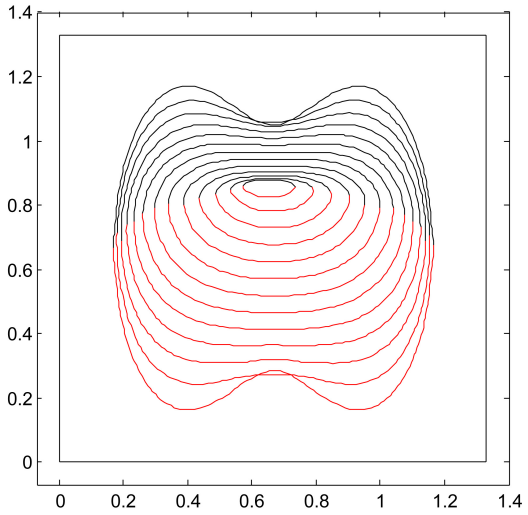

Figure 5: In this case the initial wound is a Cassini oval (parameters are $a = 1$ and $b = 1.1$). We make it evolve using equation (1) where the magnitude of f_{cable} is equal to 0.02 on the upper side (black) and to 0.04 on the lower side (red).

band once the point enters the zipping domain, i.e. for the values of i (our discrete time index) for wich our material point is in Z_i. As we described before this is motivated by experiments where the expression of proteins affecting the zipping is induced only in the engrailed (or the patched) half-segments. One such example is given in [7] where the expression of spastine, which affects fillopodia formation and activity, is modulated using an engrailed-gal4 driver. Thus, the zipping is strongly perturbed in the engrailed bands and we can obseve changes in the topology of the leading edge (see supplementary movie S7 in [7]) which, as you can see in figure 9, are also visible in our simulation.

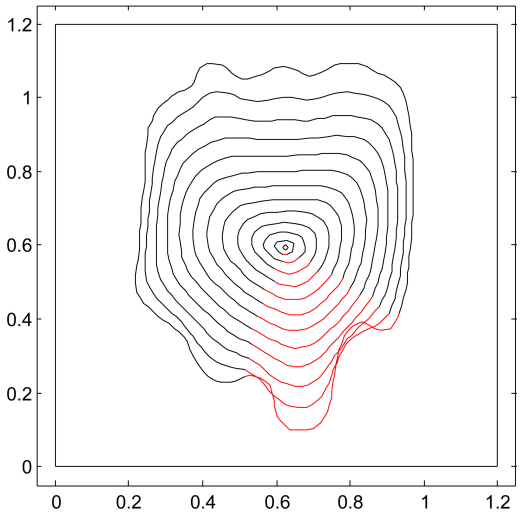

Figure 6: Initial wound is a virtual realistic curve subject to 2 deforming loads: a homogeneous cable tension (f_{cable} is equal to 0.02 everywhere), and a differentiated normal flow, exerted only on the red part ($f_{pull} = 0.03$ in the red portion of each curve and zero elsewhere).

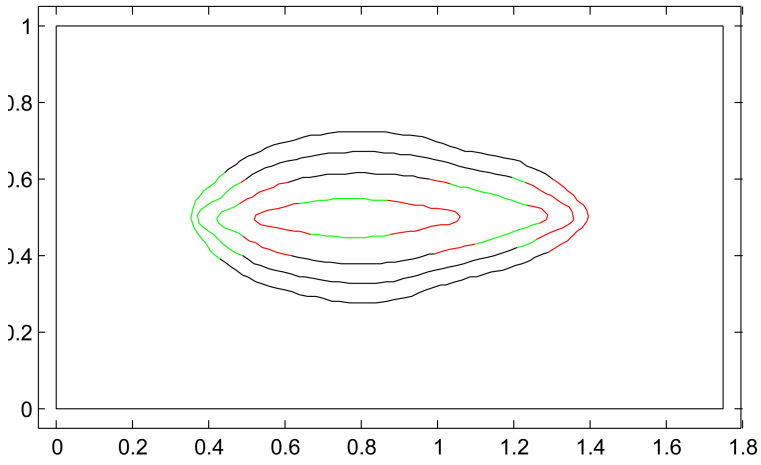

Figure 7: A quasistatic simulation of the embryonic dorsal closure of drosophila. Constant traction is exerted on the lower and upper sides of the rectangular observation area with magnitude $C_1 = 0.01$, while homogeneous mean curvature and normal flows are applied on the leading edge, with constant magnitudes of respectively $f_{cable} = 0.06$ and $f_{pull} = 0.05$. The zipping forces are uniform: $f_{zip} = 1.0$ on both the left (red portion) and the right (green portion) of the leading edge.

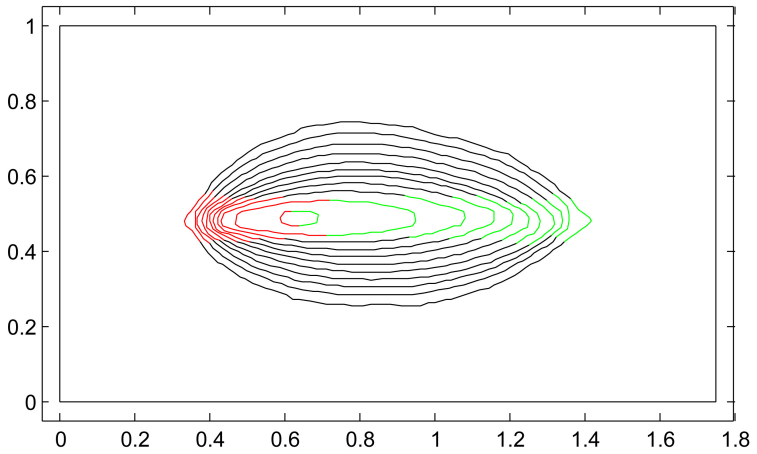

Figure 8: A quasistatic simulation of the embryonic dorsal closure of drosophila. Constant traction is exerted on the lower and upper sides of the rectangular observation area with magnitude $C_1 = 0.01$, while homogeneous mean curvature and normal flows are applied on the leading edge, with constant magnitudes of respectively $f_{cable} = 0.06$ and $f_{pull} = 0.01$. The zipping forces are differentiated along the apical axis, with magnitude $f_{zip} = 0.1$ on the left (red part) and $f_{zip} = 1.0$ on the right (green part), of the leading edge.

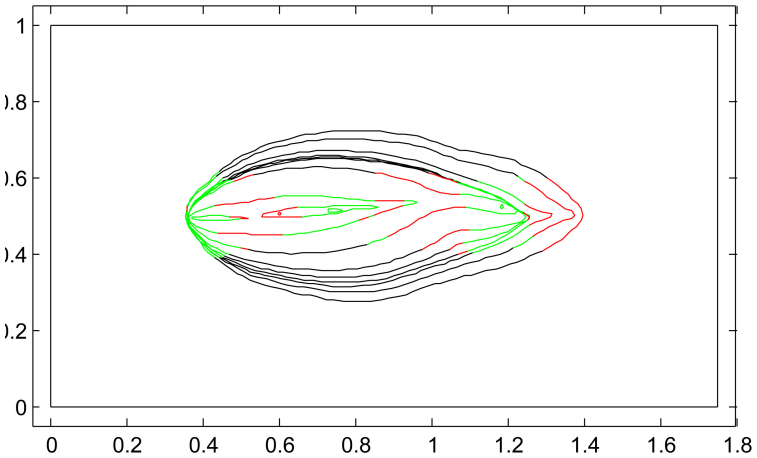

Figure 9: A quasistatic simulation of the embryonic dorsal closure of drosophila. Constant traction is exerted on the lower and upper sides of the rectangular observation area with magnitude $C_1 = 0.01$, while homogeneous mean curvature and normal flows are applied on the leading edge, with constant magnitudes of respectively $f_{cable} = 0.06$ and $f_{pull} = 0.01$. The zipping forces are differentiated along the apical axis, with magnitude $f_{zip} = 0$ on the green portions of the leading edge and $f_{zip} = 1.0$ on the red ones.

References

[1] Luís Almeida, Patrizia Bagnerini, Abderrahmane Habbal, Stéphane Noselli, and Fanny Serman. Tissue repair modeling. In *Singularities in nonlinear evolution phenomena and applications*, volume 9 of *CRM Series*, pages 27–46. Ed. Norm., Pisa, 2009.

[2] Luís Almeida, Patrizia Bagnerini, Abderrahmane Habbal, Stéphane Noselli, and Fanny Serman. A mathematical model for dorsal closure. *J Theor Biol*, 268(1):105–119, Jan 2011.

[3] Luís Almeida, Antonin Chambolle, and Matteo Novaga. Implicit scheme for mean curvature flow with obstacles. biology, 2011.

[4] Luís Almeida and Jacques Demongeot. Predictive power of "a minima" models in biology. 2011.

[5] M. Shane Hutson, Yoichiro Tokutake, Ming-Shien Chang, James W Bloor, Stephanos Venakides, Daniel P Kiehart, and Glenn S Edwards. Forces for morphogenesis investigated with laser microsurgery and quantitative modeling. *Science*, 300(5616):145–149, Apr 2003.

[6] Antonio Jacinto, William Wood, Sarah Woolner, Charlotte Hiley, Laura Turner, Clive Wilson, Alfonso Martinez-Arias, and Paul Martin. Dynamic analysis of actin cable function during drosophila dorsal closure. *Curr Biol*, 12(14):1245–1250, Jul 2002.

[7] Ferenc Jankovics and Damian Brunner. Transiently reorganized microtubules are essential for zippering during dorsal closure in drosophila melanogaster. *Dev Cell*, 11(3):375–385, Sep 2006.

[8] Ron Kimmel. *Numerical geometry of images*. Springer-Verlag, New York, 2004.

[9] Anita T Layton, Yusuke Toyama, Guo-Qiang Yang, Glenn S Edwards, Daniel P Kiehart, and Stephanos Venakides. Drosophila morphogenesis: tissue force laws and the modeling of dorsal closure. *HFSP J*, 3(6):441–460, Dec 2009.

[10] Adam C Martin, Matthias Kaschube, and Eric F Wieschaus. Pulsed contractions of an actin-myosin network drive apical constriction. *Nature*, 457(7228):495–499, Jan 2009.

[11] Paul Martin and Susan M Parkhurst. Parallels between tissue repair and embryo morphogenesis. *Development*, 131(13):3021–3034, Jul 2004.

[12] Ian M. Mitchell. The flexible, extensible and efficient toolbox of level set methods. *J. Sci. Comput.*, 35(2-3):300–329, 2008.

[13] S. Osher and Chi-Wang Shu. High-order essentially nonoscillatory schemes for hamilton-jacobi equations. *SIAM J. Numer. Anal.*, 28(4):907–922, 1991.

[14] Jerome Solon, Aynur Kaya-Copur, Julien Colombelli, and Damian Brunner. Pulsed forces timed by a ratchet-like mechanism drive directed tissue movement during dorsal closure. *Cell*, 137(7):1331–1342, Jun 2009.

[15] Yusuke Toyama, Xomalin G Peralta, Adrienne R Wells, Daniel P Kiehart, and Glenn S Edwards. Apoptotic force and tissue dynamics during drosophila embryogenesis. *Science*, 321(5896):1683–1686, Sep 2008.

[16] William Wood, Antonio Jacinto, Richard Grose, Sarah Woolner, Jonathan Gale, Clive Wilson, and Paul Martin. Wound healing recapitulates morphogenesis in drosophila embryos. *Nat Cell Biol*, 4(11):907–912, Nov 2002.